Optimisation of Electrical Impedance Tomography Image Reconstruction Error Using Heuristic Algorithms

Talha A. Khan*[a], Sai Ho Ling[b], Arslan A. Rizvi[c]

[a]*Department of Tech & Software, University of Europe for Applied Sciences, Think Campus, Konrad-Zuse-Ring 11, 14469 Potsdam, Germany*
[b]*Department of Biomedical Engineering, University of Technology Sydney, Sydney, Australia*
[c]*State Key Laboratory of Multiphase Flow in Power Engineering, Xi'an Jiaotong University, 28 Xianning West Road, Xi'an 710049, Shaanxi, China*

Abstract:

Preventing living tissues' direct exposure to ionising radiation has resulted in tremendous growth in medical imaging and e-health, enhancing intensive care of perilous patients and helping to improve quality of life. Moreover, the practice of image-reconstruction instruments that utilise ionising radiation significantly impacts the patient's health. Prolonged or frequent exposure to ionising radiation is linked to several illnesses like cancer. These factors urged the advancement of non-invasive approaches, for instance, Electrical Impedance Tomography (EIT), a portable, non-invasive, low-cost, and safe imaging method. EIT image reconstruction still demands more exploitation, as it is an inverse and ill-conditioned problem. Numerous numerical techniques are used to answer this problem without producing anatomically unpredictable outcomes. Evolutionary Computational techniques can substitute conventional methods that usually create low-resolution blurry images.

EIT reconstruction techniques optimise the relative error of reconstruction using population-based optimisation methods presented in this work. Three advanced optimisation methods have been developed to facilitate the iterative procedure for avoiding anatomically erratic solutions. Three different optimising techniques, namely, a) Advanced Particle Swarm Optimisation Algorithm (APSO), b) Advanced Gravitational Search Algorithm (AGSA), and c) Hybrid Gravitational Search Particle Swarm Optimization Algorithm (HGSPSO), are used. The convergence and solution stability performance is improved by utilising the advantages of these proposed techniques.

EIT images were obtained from the EIDORS library database for two case studies. The image reconstruction was optimised using the three proposed algorithms. EIDORS library was used for generating and solving forward and reversed problems. Two case studies were undertaken, i.e. circular tank simulation and gastric emptying. Thus, the results are analysed and presented as a real-world application of population-based optimisation methods.

Results obtained from the proposed methods are quantitatively assessed with ground truth images using the relative mean squared error, confirming that a low error value is reached in the results. The HGSPSO algorithm performs better than the other proposed methods regarding solution quality and stability.

Keywords: Electrical Impedance Tomography, Advanced PSO, Image Reconstruction

Nomenclature

PSO	**Particle Swarm Optimisation**	**FEM**	**Finite Element Method**
EIT	**Electrical Impedance Tomography**	**GSA**	**Gravitational Search Algorithm**
HGSPSO	**Hybrid Gravitational Search Particle Swarm Optimization**		

1 Introduction

Over the years, the progress and practice of non-invasive imaging methods in biology and medicine have been drastically enhanced due to industry and academic collaboration. The hazardous radiations produced by these imaging devices cause significant health problems for exposed patients [1]. These radiations can yield medium to severe illnesses such as cancer, a universal health concern. Electrical impedance tomography (EIT), a non-invasive imaging method, injects a low amplitude current on the body's surface and calculates the voltage on the surface electrodes. These voltage measurements are used as inputs to solve an inverse problem to recuperate the object's internal electrical properties (permittivity and conductivity) under examination [2]. EIT is a low-cost imaging method with no identified hazards; therefore, it has numerous industrial and medical applications. Image reconstruction is regarded as an ill-conditioned nonlinear inverse problem in EIT that requires an efficient reconstruction method proficient in handling complex boundary shapes, noise in the measured data, and electrode locations. Because of being an ill-conditioned problem, the image reconstructed often has a low spatial resolution. A slight variation in the measured voltages causes a massive change in the conductivity or permittivity [3]. EIT is a two-step problem, the first stage is the forward problem, and the second stage is the inverse problem [4].

1.1 Mathematical Modelling of Forward Problem

The forward problem solution contains the voltage measurements on the surface electrodes for specific conductivity or resistivity distribution; however, the given object's applied current and conductivity distribution are known [5]. The finite Element Method (FEM) is used to acquire the numerical solution. To get the measured voltages at the electrodes forward problem has to be solved in EIT simulations. Mathematically EIT is represented by the Poison equations, which are as follows [6].

$$\nabla.[\sigma(\vec{u})\nabla\emptyset(\vec{u})] = 0, \ \forall\vec{u} \in \Omega \tag{1}$$

$$\emptyset_{sur}(\vec{u}) = \emptyset(\vec{u}), \forall\vec{u} \in \partial\Omega \tag{2}$$

$$I(\vec{u}) = -\sigma(\vec{u})\nabla\emptyset(\vec{u}) \cdot \hat{n}(\vec{u}), \quad \forall\vec{u} \in \partial\Omega \tag{3}$$

where $I(\vec{u})$ is the electrical current, $\emptyset(\vec{u})$ is the general distribution of electrical potentials, Ω is the volume of interest, also called the domain, $(\vec{u}) = (x, y, z)$ is the position of the object under study, $\emptyset_{sur}(\vec{u})$ is the distribution of electric potentials on surface electrodes, $\sigma(\vec{u})$ is the distribution of electrical conductivities, $\partial\Omega$ is the boundary of the domain, and $\hat{n}(\vec{u})$ is the normal surface vector in position $(\vec{u}) \in \partial\Omega$.

To determine the electric potential at the surface of the electrodes by applying current and given conductivity distribution following relationship is used.

$$\emptyset_{sur}(\vec{v}) = f(I(\vec{v}), \sigma(\vec{v})), \forall\vec{v} \in \partial\Omega \ \wedge (\vec{u}) \in \Omega \tag{4}$$

To find out the conductivity distribution from the $I(\vec{u})$ and $\emptyset_{sur}(\vec{u})$ is called the inverse problem is given by the following mathematical expression:

$$\sigma(\vec{u}) = f^{-1}((I(\vec{v}), \emptyset_{sur}(\vec{v})), \quad \forall\vec{v} \in \partial\Omega \ \wedge (\vec{u}) \in \Omega \tag{5}$$

1.2 Mathematical Modelling of Inverse Problem

EIT inverse problem focuses on determining the electrical properties of the object, which are dependent on the voltage measurements recorded at the surface of the domain [7]. The testing object placed in the volume conductor may vary in size. In EIT, the inverse problem is a complex problem involving many aspects. The nonlinearity of the problem is not the only reason. Still, it is severely ill-conditioned, which means a minor difference in the electrical conductivity of the medium can bring a massive variation in measured electrical potential at the domain's boundaries. According to the theoretical perspective, the measured potential attained from the boundaries can be associated with a single conductivity distribution; however, the limited number of available measurements changes in real applications, making it different from the theoretical assumption. Other methods were presented for tackling the inverse nature of EIT. These methods can be separated into various types: inverse solvers that are nonlinear iterative methods such as linear approximators, Artificial Intelligence (AI) based techniques, Primal-Dual Interior Point Method (PDIPM), and Bayesian approach.[7]

The linear approximation methods, for instance, one-step Gauss-Newton (GN), depend on a priori information and consider conductivity variation behaviour linear. While taking the measurements using linear algorithms, the most common setback is the linear change of the conductivity at the boundary of the objects, which leads to the strenuous evaluation of the target object. However, these methods can be beneficial in minimising the noise in data calculations. These algorithms are proficient in some particular applications; however, for nonlinear inhomogeneity, they cannot converge to the exact conductivity distribution [8]. On the contrary, nonlinear iterative techniques, such as the PDIPM, consider the nonlinearity and ill-condition of the inverse problem of EIT and use verified advanced computational methods to optimise nonlinear problems. Such a case was studied by Borsic et al. [9], who solved the EIT problem using the iterative PDIPM method. Although these methods can give an improved approximation compared to the linear algorithms, require more computational time and are sensitive to noise. Hence, nonlinear iterative algorithms do not apply to actual EIT applications. The Bayesian inversion approach modelled the conductivity distribution as a random variable that obeys a prior density function and a posterior probability density that holds existing information of the conductivity distribution [10], i.e. *a priori* conductivity distribution is used to solve the inverse problem. The posterior density is the comprehensive probabilistic model of the EIT problem and characterises the vagueness in the unknown variables for available measurements. AI-based techniques such as Neural Networks [11]and evolutionary methods [12] were also employed for the EIT inverse problem. These methods are self-sufficient to determine the solution steps for solving the inverse EIT problem. The learning phase is carried out by associating a set of potential measurements and their relative conductivity distribution. They guess the conductivity distribution from the measurements after the learning phase. AI-based techniques are proficient in estimating the conductivity distribution in low computational time and, consequently, are appropriate for real-time applications [13]. After creating the data required for training that comprises noise and several artefacts, these algorithms can perform well in reconstructing the conductive distribution.

1.3 Main Contributions to this Work

The focus of this study is to use the advanced heuristic algorithms, which the authors have developed and published [14–16] This work implements two cases based on the reconstruction of EIT images from EIDORS. The authors have used these advanced optimisation algorithms to reduce the reconstruction error of the EIT images. The primary purpose of optimisation algorithms is to achieve a final reconstructed image with the least reconstruction error.

2 Optimisation Methodology for EIT Reconstruction

The boundary domain is discretised into the small elements in a closed area to solve the problem. Hence, Ω and ∂Ω have a fixed number of meshes. Let us assume that n_a is the number of the meshes in the closed region such that n_a = Ω and n_b is the number of meshes at the boundary such that n_b = ∂Ω; the error fitness function is expressed as:

$$e_k = \sum_{i=1}^{n_b} (U_i(x_k) - V_i)^2 \quad (6)$$

where $V = [V_1\, V_2\, V_3 \ldots V_{n_b}]$ is the measured potential at the boundary of the domain, $U(x_k) = [U_1(x_k), U_2(x_k), U_3(x_k), \ldots U_{n_b}(x_k)]^T$ is the calculated potential.

The inverse problem of EIT is solved by reducing the fitness function between the measured and expected electric potential values. The dimensions of the search area in the EIT inverse problem are equal to the number of meshes of the finite element model. For implementing the population-based optimisation algorithms for this inverse problem, the vector x_k denotes the *l*-dimensional conductivities values, where *l* is the number of meshes of the FE model. The i^{th} member of a population's position is represented as $x_k = [x_{k1}, x_{k2}, \ldots, x_{kl}] = [\sigma_{k1}, \sigma_{k2}, \ldots, \sigma_{kl}]$, where σ_{k1} is the conductivity value of the first element, and so on. Therefore,

$$U(x_k) = U(\sigma_k) = f(I(\vec{u}), \sigma_k) \quad (7)$$

The fitness function "*r*" is defined as the relative square error (Eq. 8) for solving the EIT inverse problem.

$$r(x) = r(\sigma) = \left[\frac{\sum_{i=1}^{n_b}(U_i(x) - V_i)^2}{\sum_{i=1}^{n_b} V_i^2}\right]^{1/2} \quad (8)$$

The EIT reconstruction problem can be treated as finding the optimal conductivity distribution, *σ*, such that the error function, $r(x)$ is minimum. This study uses population-based optimisation methods to solve the EIT reconstruction problem.

2.1 Proposed Methodologies:

The authors developed the following algorithms, which are briefly described and used in this paper for solving the EIT problem. A detailed explanation of all these three algorithms can be found in [14–16]

2.1.1 Advanced Particle Swarm Optimisation Algorithm (APSO):

The conventional PSO method is essentially based on two equations: particle position and particle velocity. The APSO employed adds a term to the velocity equation, enhancing the PSO's performance.

a) Modification in the velocity update equation:

The advanced PSO employs the same initialisation process and parameters as the Standard PSO. The key distinction is in the velocity equation, which is also a critical component of the PSO algorithm. The third factor introduced into the PSO's velocity equation minimises particle positions during iterations, increasing velocity and allowing the algorithm to achieve the optimal solution faster. Furthermore, the particle position is influenced by the inertia weight. The velocity and position equations will be

$$v_i = wv_i + c_1R_1(p_i - x_i) + c_2R_2(p_g - x_i) + w\left(\frac{c_1}{c_2}\right)(p_i - p_g) \quad (9)$$

$$x_i(t+1) = wx_i(t) + v_i \quad (10)$$

The new method used different equations and approaches to determine the particle's new position and velocity. As previously stated, the fitness test will find the local and global best in the same manner that the conventional PSO does. The rationale for dividing C_1 and C_2 in the velocity updated equation in the modified term is to keep the value from too little or too big, as both acceleration constants substantially influence particle movement in the search space. A nominal value aids particle convergence towards the optimal solution.

b) Important Parameters Selection for the proposed algorithm:

Several aspects were taken into account when developing the APSO algorithm. These variables include the inertia constant, acceleration constants, and the maximum velocity limit.

i. Maximum Velocity Selection:

The APSO method assesses the velocity and location of each swarm member as they move in the provided search space dimensions after each iteration. If the value is enormous, members of the swarm can move unsteadily and far away from the best solution; on the other hand, if it is minimum, the particle's mobility is limited and does not move towards the best solution.

ii. Acceleration constants Selection:

The velocity equation's acceleration constants control the movements of every swarm member as it approaches the global and local optimal positions. If the values of the acceleration constants are too little, the movement of each component will be reduced. If it is too huge, each part deviates from its location. The acceleration constants are frequently used to fulfil the condition $C_1+C_2 \leq 4$. PSO generally does not converge if it does not satisfy $C_1+C_2 \leq 4$. Therefore, APSO's C_1 and C_2 values are set to 2.1 and 1.9, respectively.

iii. Selection of inertia constant:

The inertial weight "*w*" is a crucial parameter to examine the convergence behaviour of the proposed APSO. The influence of the initial velocity on the present update is controlled by inertial weight. Inertial weight is a trade-off between the swarm's global and local capabilities. If the inertial weight has a higher value, it will enhance global exploration, i.e. it will aid in the search for new places. Similarly, suppose the inertial weight is minimal. In that case, it will facilitate local exploration, i.e. it will help fine-tune the present search region. As a result, in APSO, the inertial weight decreases linearly from one iteration to the next. The following relation is being used for inertial weight control:

$$\chi = \frac{2}{\Phi - 2 + \sqrt{\Phi^2 - 4*\Phi}} \tag{11}$$

$$w = \chi * \left(0.0005 + w * \left(\frac{T-(t-30)}{T}\right)\right) \tag{12}$$

In eq (12), *T* is the total iteration. The constriction factor is calculated as follows when *phi*=4.1; This constriction factor is used to modify inertial weight. The following control is incorporated into the inertial weight. In this paper, the value of *phi* is constant at 4.1.

2.1.2 Advanced Gravitational Search Algorithm (AGSA)

The masses of agents assess the performance of the proposed approach. In AGSA, the force of gravity draws all agents. It is responsible for their movement toward the agents with greater mass. Higher mass agents are considered the best solution to the given problem. Since the physics laws inspire AGSA, every agent has four characteristics these are passive gravitational mass "M_p", inertial mass "M_i", active gravitational mass "M_a", and position. Let's consider a system having "*N*" agents; the position of the i^{th} agent can be defined as:

$$X_i = X_i^1 + X_i^2 + \cdots + X_i^d + X_i^n \ \ for\ i = (1,2,\dots,N) \tag{13}$$

In the d^{th} dimension, "*N*" denotes the dimension of the search area and "x^d" represents the position of the i^{th} object. The force exerting on mass "*i*" from mass "*j*" at time *t* is defined as:

$$F_{ij}^d(t) = G(t)\frac{M_{pi}(t)\times M_{aj}(t)}{R_{ij}(t)+\epsilon}\left(X_j^d(t) - X_i^d(t)\right) \tag{9}$$

where *G(t)* is a gravitational constant at time *t*, $R_{ij}(t)$is the distance between two objects *i* and *j*, and ε is a small constant. M_{pi} is the passive gravitational mass related to object *i*. M_{aj} is an active gravitational mass of object *j*.

Let's assume that in dimension *d*, the total force acted on object *i* is a random weighted sum of all the components of the forces applied on the other agents. Then (14) can be rewritten as:

$$F_i^d(t) = \sum_{j=1, j\neq i}^{N} rand_j\, F_{ij}^d(t) \tag{10}$$

Defined by the second law of motion at time t, the acceleration of the object *i* in the direction d can be written as:

$$a_i^d(t) = \frac{F_i^d(t)}{M_{ii}(t)} \tag{11}$$

For the i^{th} agent, M_{ii} is the inertial mass. The velocity of the agents is based on acceleration and their present velocity. The position and the velocity of every agent are updated by (17) and (18) as

$$X_i^d(t+1) = X_i^d + v_i^d(t+1) \tag{12}$$

$$v_i^d(t+1) = \left(rand_i \times v_i^d(t) + a_i^d(t)\right) \times \left(1 - \frac{t}{T}\right)^{\alpha} \tag{13}$$

where $rand_i$ is a uniform random number within [0-1], *t* is the current iteration, *T* is the total number of iterations, which is the stopping criteria, and α is an integer. The gravitational constant, *G*, monitors the searching accuracy, decreasing over the iteration. In AGSA, the inertial and gravitational masses are calculated by evaluating the fitness function. An agent with heavier masses is efficient and indicates that agents with heavier masses have higher attractions and move slowly. Suppose all the masses are equal so the inertial mass and the gravitational masses can be updated as follows:

$$M_{ai} = M_{ii} = M_{pi} = M_i \quad i = 1,2,3,\dots\dots\dots N \tag{14}$$

$$m_i(t) = \frac{fit_i(t) - X^w(t)}{X^b(t) - X^w(t)} \tag{20}$$

$$M_i(t) = \frac{m_i(t)}{\sum_{j=1}^{N} m_j(t)} \tag{21}$$

At time *t*, *fiti (t)* is the fitness value of the agent. Worst $X^w(t)$ and Best $X^b(t)$ for a maximisation problem are defined as:

$$X^b(t) = \max_{j\varepsilon\{1,\dots N\}} fit_j(t) \tag{22}$$

$$X^w(t) = \min_j \varepsilon\{1, \dots N\} \text{ fit } (t) \tag{23}$$

For the minimisation problem, (22) and (23) are defined as follows:

$$X^b(t) = \min_j \varepsilon\{1, \dots N\} \text{ fit } (t) \tag{15}$$

$$X^w(t) = \max_{j\varepsilon}\{1, \dots N\} \text{ fit } _j(t) \tag{16}$$

The number of agents is gradually reduced to maintain a balance between exploration and exploitation in AGSA until only agents with larger masses applying gravity to the other agents in the search space are considered. This set of agents is called the best agents, "K_{best}." As a result, the value of K_{best} gradually decreases over iterations until just one agent applies force to the other agents. As a result, (15) is changed as follows:

$$F_i^d(t) = \sum_{j\varepsilon K_{best}, j\neq \mathrm{i}} \mathrm{rand}_j \ F_{ij}^d(t) \tag{17}$$

2.1.3 Hybrid Gravitational Search Particle Swarm Optimization Algorithm (HGSPSO)

In the literature, several hybrid algorithms employ the qualities of two or more algorithms to increase the proficiencies of the hybrid variants. At the low and high levels, several techniques are utilised to merge the two methods in a homogeneous and heterogeneous manner. GSA is combined with PSO in this study, and the properties of both algorithms are used, i.e. both methods were conducted concurrently, and the hybrid algorithm, HGSPSO, is used to produce the results. The proposed fusion is primarily motivated by the need to capitalise on the PSO's exploitation capabilities and the GSA's exploration expertise. The parameters of each of these algorithms are used in HGSPSO. The two most significant parameters in PSO are the inertial weight and acceleration constants. As a result, in HGSPSO, inertial weight "w" is adjusted to either not employed as a linear reduction or is set as a constant value. However, it is used as a function of the global and local best fitness function values. Similarly, as the iteration advances, the acceleration constants utilised in this study vary adaptively. These two parameters are defined as follows:

$$w_i = 1 - \left(\frac{p_g}{p_i}\right) \tag{18}$$

$$C_1 = (C_3 - C_4) * \left(1 - \frac{t}{T}\right) + C_4 \tag{19}$$

$$C_2 = (C_5 - C_6) * \left(1 - \frac{t}{T}\right) + C_6 \tag{20}$$

where C_3, C_4, C_5, and C_6 are constants values, "T" is the maximum iteration, and "t" is the current iteration. C_1 values decrease adaptively, whereas C_2 values increase during the iteration. Therefore, as the proposed approach advances to the exploitation stage, the masses become closer to the optimal solution. The acceleration coefficients are adjusted adaptively because there is no boundary in the evolutionary computation for transiting between these two phases. Furthermore, this adaptive technique aids exploration in the early stages and exploitation in the latter stages. The HGSPSO produces the best results when C_1 is reduced from 2.5 to 0.5, C_2 is reduced from 0.5 to 2.5, p_g is the global best, and p_i is the local best. Every agent is regarded as a potential solution in HGSPSO. Among other agents, the gravitational constant and gravitational force are measured using (30) and (31). (33) computes the agents' acceleration. At the time "t", the force of attraction by agent (mass) "i" from an agent (mass) "j" is defined as:

$$F_{ij}^d(t) = G(t)\frac{M_{pi}(t) * M_{aj}(t)}{R_{ij}(t) + \varepsilon}\left(X_j^d(t) - X_i^d(t)\right) \tag{30}$$

where Mp_i is the passive gravitational mass associated with object i, ε is a small constant, $Rij(t)$ is the distance between two agents i and j, Ma_j is an active gravitational mass of agent j, and $G(t)$ is a gravitational constant at time t. G has been utilised adaptively to represent the relevance of exploration in the early stages of the algorithm and exploitation in the later stages. As a result, its value increases with each iteration. The primary goal of creating the G adaptively is to encourage the agents to take larger steps in the early stages of the algorithm. However, agents are compelled to travel gradually by the end of the iterations. (t) is modified as follows:

$$G(t) = G_o \times e^{-\gamma \times \left(\frac{T-t}{T}\right)} \tag{31}$$

where G_o is the initial gravitational constant and γ is the coefficient of decrease. Assume that in dimension "D", the overall force experienced on agent i is a random weighted sum of all the other parts of the forces exerted on the other agents (26) can be modified by the following equation.

$$F_i^d(t) = \sum_{j=1, j\neq \mathrm{i}}^{N} \mathrm{rand}_j \ F_{ij}^d(\mathrm{t}) \tag{32}$$

Similarly, acceleration can be calculated as

$$a_i^d(t) = \frac{F_i^d(t)}{M_{ii}(t)} \tag{33}$$

For the minimisation problem, the gravitational and inertial masses may be calculated similarly defined from (19-21). As previously stated, the GSA is a memoryless algorithm. The optimal solution may not be saved because other less-fitted masses pull away the best mass. A novel velocity update technique is proposed to circumvent this issue. The updated velocity update equation is as follows:

$$v_i(t+1) = w \times v_i(t) + c_1 \times a_i + \frac{c_1}{c_2} \times (p_g - p_i) \tag{21}$$

Where C_1 and C_2 are the acceleration constants, w is the inertial weight, a is the acceleration, p_g is the global best (gbest), p_i is the local best position, and v_i is the agent's velocity. The third term in (34) is similar to the social element in the PSO velocity equation. A greater C_1 value favours GSA behaviour, whereas a more significant C_2 value favours PSO's social aspect in the search method's execution. The adaptive approach allows GSA to evaluate the search region more effectively, and a PSO exploits the best solution. Finally, the positions of agents are modified as follows:

$$X_i^d(t+1) = w \times X_i^d + v_i^d(t+1) \tag{22}$$

All agents are randomly initialised in the proposed algorithm. Particle acceleration is then measured by utilising (33). At each iteration, the best solution found thus far should be updated. The velocities of all agents are then computed using (30), and the agents' locations are finally updated using (35). The iterations are completed when the required stopping criteria are met.

3 Applications for EIT

To study the EIT problem, two cases are used. In case 1, a circular tank simulation is conducted using the EIDORS [17]. In the second case, a gastric emptying problem is studied, and images are reconstructed using the data available in EIDORS.

3.1 Circular Tank Simulation by using EIDORS

To assess the performance of the proposed methods, a circular tank simulation is conducted by creating the forward model from EIDORS. The simulations are performed by implementing a 16-electrode EIT system. The forward modelling is achieved by the finite element method by discretising the forward model into small elements called meshes. The EIDORS parameters for the forward modelling are set as refining level '*2*' and density level '*b*'. In this work, the detection of irregular objects is obtained that are placed at three different locations inside the circular tank. The relative error amongst the distributions of calculated and measured electrical potentials at the domain boundary is utilised from the optimisation perspective. The dimension of the problem is equal to the number of meshes of the finite element model. Each candidate's solution is the real vector used as a possible conductivity distribution. The population size of each algorithm is set to 100 agents. The stopping criteria are placed until the best image is obtained or when the total number of iterations is obtained. The images were obtained at t=50, 100, 200, 300, 400, and 500 iterations. The fitness function assesses the evaluation of the performance of the proposed methods.

3.1.1 Experiential setup

The experimental model was made to simulate the cylindrical phantom problem of EIT imaging and optimise the image reconstruction quality using swarm intelligence. The model consists of a cylindrical object. The interior of the cylinder has a constant and uniform conductivity. The cylinder is filled with a saline solution to achieve continuous and consistent conductivity in the physical setup. The cylinder is surrounded by 16 electrodes placed at equal arc lengths from each other. The electrodes are considered lossless, i.e., no voltage drop occurs at the electrodes and the wires connecting those electrodes. In a hardware implementation, the losses associated with electrodes and wires are also considered due to the high sensitivity of the measuring equipment.

The 16 electrodes are chosen to obtain a good image while reducing the computational cost. The number of electrodes may be increased if a better image resolution is desired. Still, the time it takes to obtain an optimum solution will increase drastically.

The inner cylinder is modelled as having a constant conductivity. A region is defined inside the domain of the outer cylinder with a constant conductivity which contrasts with the conductivity of the fluid-filled outer cylinder. Fig 1. shows the experimental simulation setup for the cylinder phantom problem.

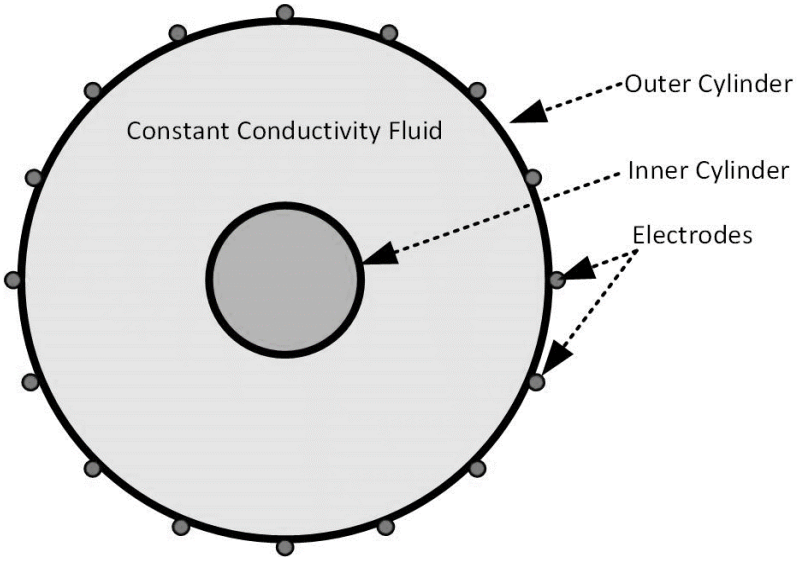

Figure 1 Experimental Model for Simulation of Cylinder Phantom Problem

3.1.2 Results and Discussion

A simulation experiment is performed to validate the efficacy of the presented reconstruction algorithms for EIT image reconstruction. The parameters adopted for conducting the simulations for the three proposed algorithms are defined in Table 1.

Table 1 Parameters of the proposed methods used for Case 1

Algorithms	**Parameters**
HGSPSO	Population size= 100, C_1 = [2.5-0.5], C_2= [0.5-2.5], w= (5.16), G_o=100
APSO	Population size=100, C_1 = [2.5-0.5], C_2= [0.5-2.5], w= (3.29)
AGSA	Population size=100, G_o=100

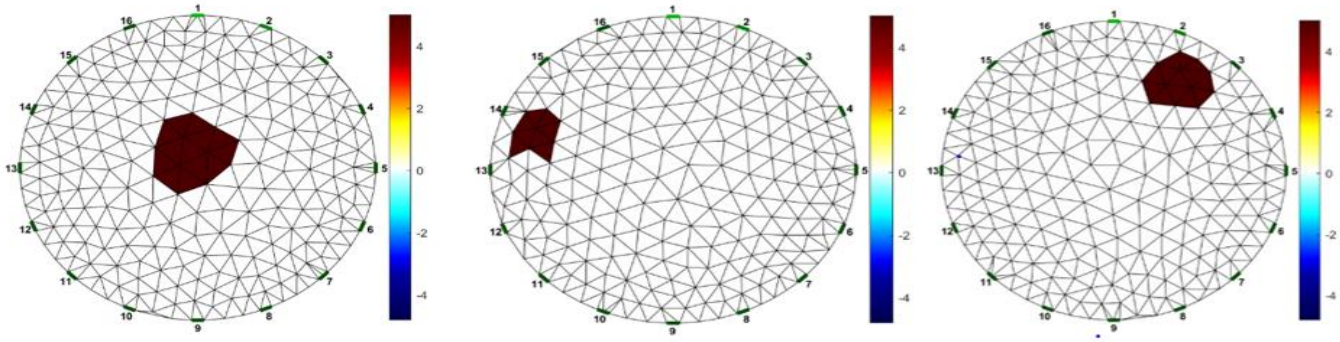

Figure 2 Forward model placed at the (i) centre (ii), near the left border (iii), and the right border of the circular domain

Figure 2 shows the forward model of the circular tank that is discretised into small elements. Each element has a conductivity value. The background conductivity is defined as 1 S/m, and the target conductivity is 6 S/m in meshes, as shown in Fig.2.

This object is highlighted with the dark colour in the forward model placed at the (*i*) centre (*ii*), near the left border (*iii*), and the right boundary of the circular domain. Figures 3, 4, and 5 show the reconstruction results obtained using APSO, AGSA, and HGSPSO algorithms. Figures 6, 7, and 8 show the RMS error with the number of iterations for the object placed in the centre, near the left border, and the right boundary of the circular domain. The performance of the reconstruction methods can be evaluated by studying the visual results shown in Figure 3, Figure 4, and Figure 5.

AGSA algorithm shows an interesting behaviour because the results attained for the initial fifty epochs are neither conclusive nor anatomically steady. Also, the error of reconstruction for all three cases is steady, and the AGSA algorithm does not further down the reconstruction error. However, from the start, APSO gives morphologically stable results for all three cases, as seen in Figures 3,4 and 5. Similarly, the relative error convergence is much better than the AGSA algorithm. Nevertheless, the HGSPSO approach gives remarkable results for all three qualitative and quantitative cases, as shown in figures 3-5. Combining the APSO and AGSA algorithms helps the HGSPSO algorithm provide the anatomically correct solution in the early iterations. It helps to escape from the

local minima, accelerating convergence quickly compared to the other two algorithms. For the object on the right side of the circular domain case, the HGSPSO algorithm minimises the error after reaching 400 iterations than the other two algorithms.

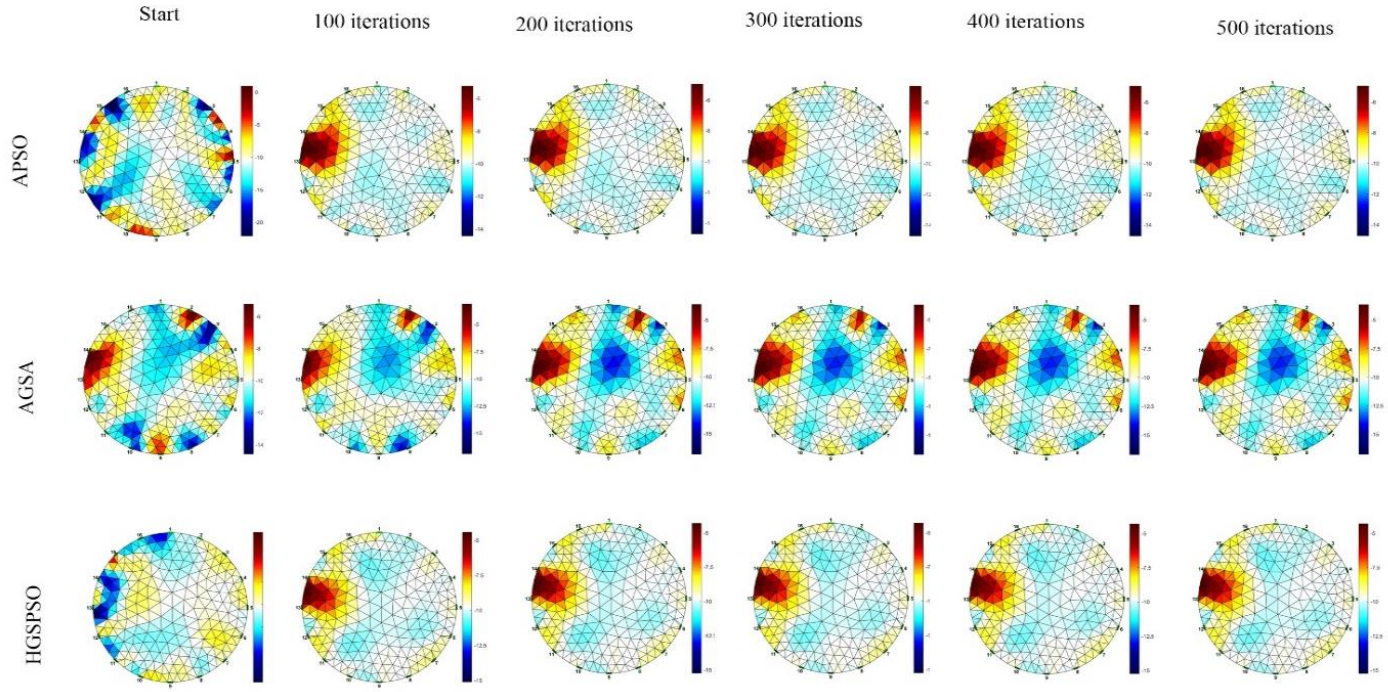

Figure 3 Reconstruction results for an object placed at the left for (A) APSO, (B) AGSA and (C) HGSPSO

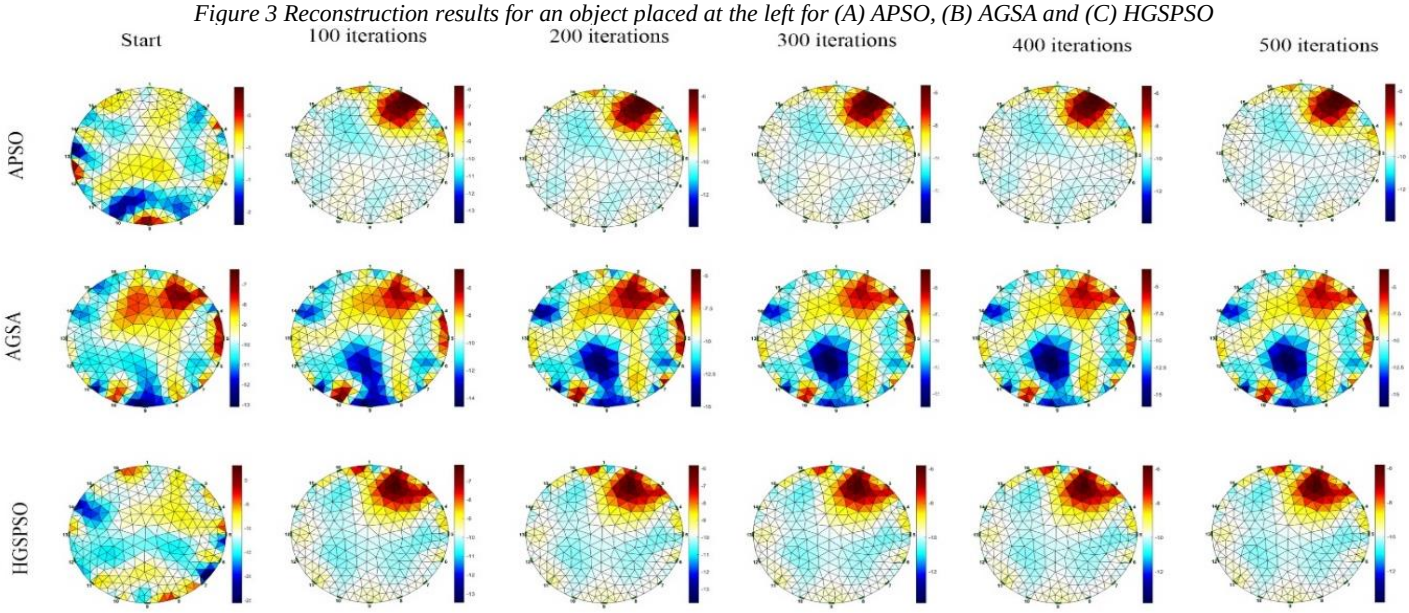

Figure 4 Reconstruction results for an object placed at the right side of the border for (A) AGSA, (B) APSO and (C) HGSPSO

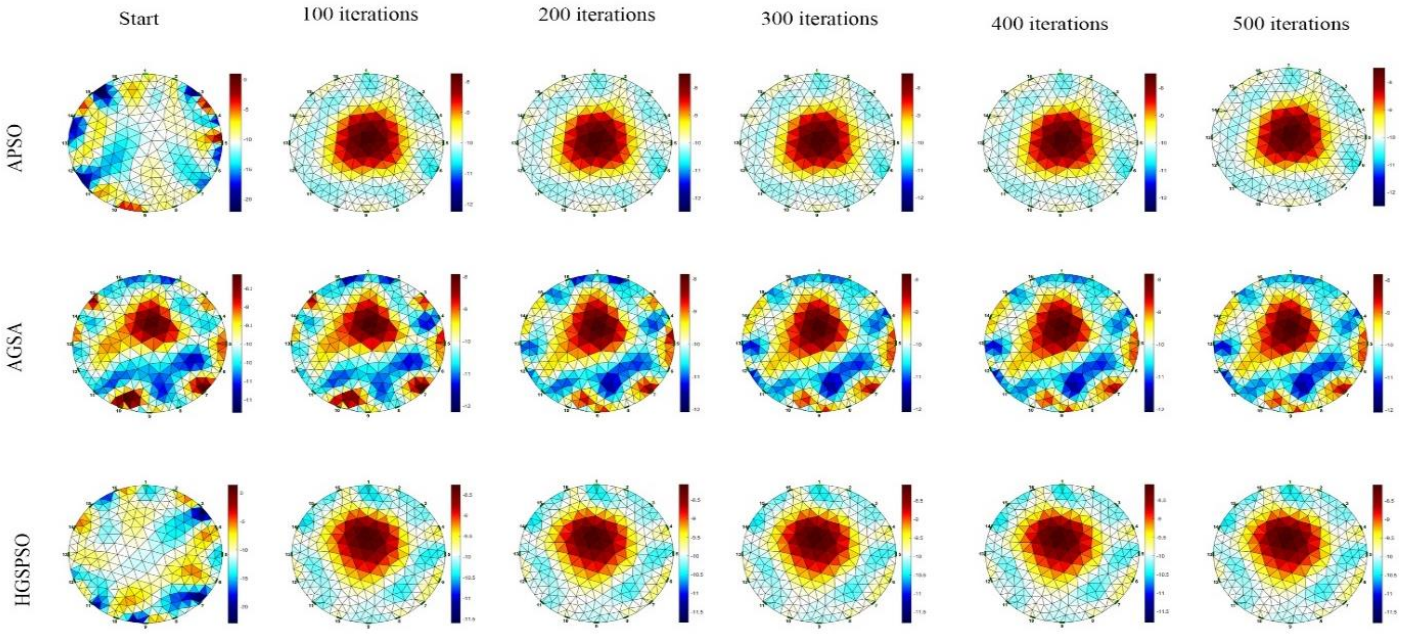

Figure 5 Reconstruction results for an object placed on the centre for (A) APSO, (B) AGSA and (C) HGSPSO

Figures 6-8 show the error reconstruction plots for all three cases, and it can be seen that the HGSPSO gives better performance than the APSO and AGSA methods. The relative error value for the HGSPSO is much smaller than the other algorithms. This RMSE replicates the reconstruction quality with relatively high sensitivity. This error lies between 0 and 1. The lesser value of the error shows that the variation between the model and the reconstructed image is small, the reconstruction quality is excellent and vice versa. If RMSE=0, that means there is no error in reconstruction.

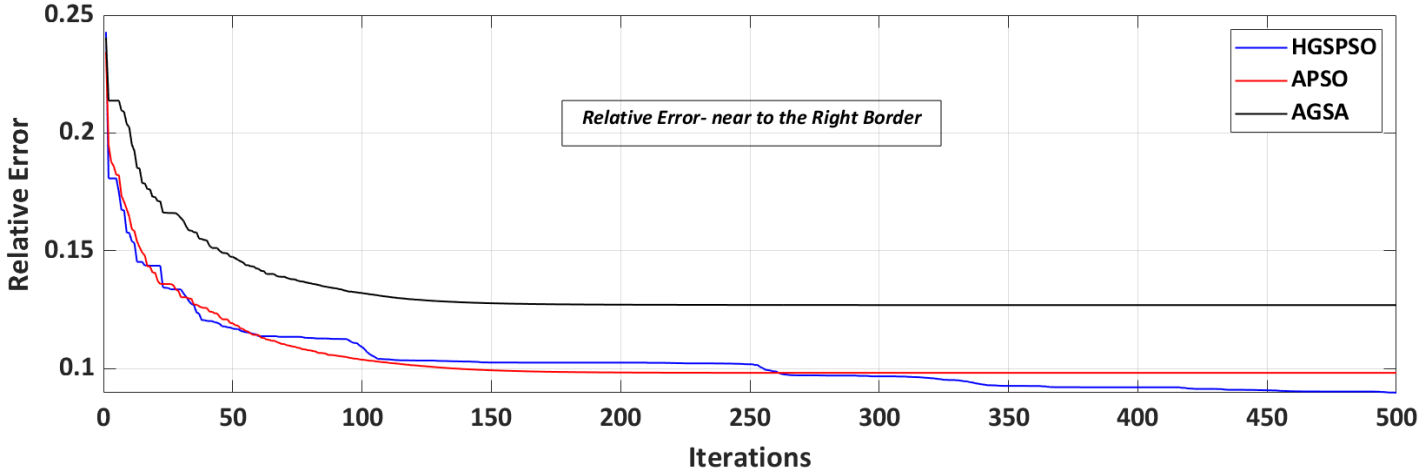

Figure 6 Error of reconstruction w.r.t iterations for an object placed at the right side of the circular

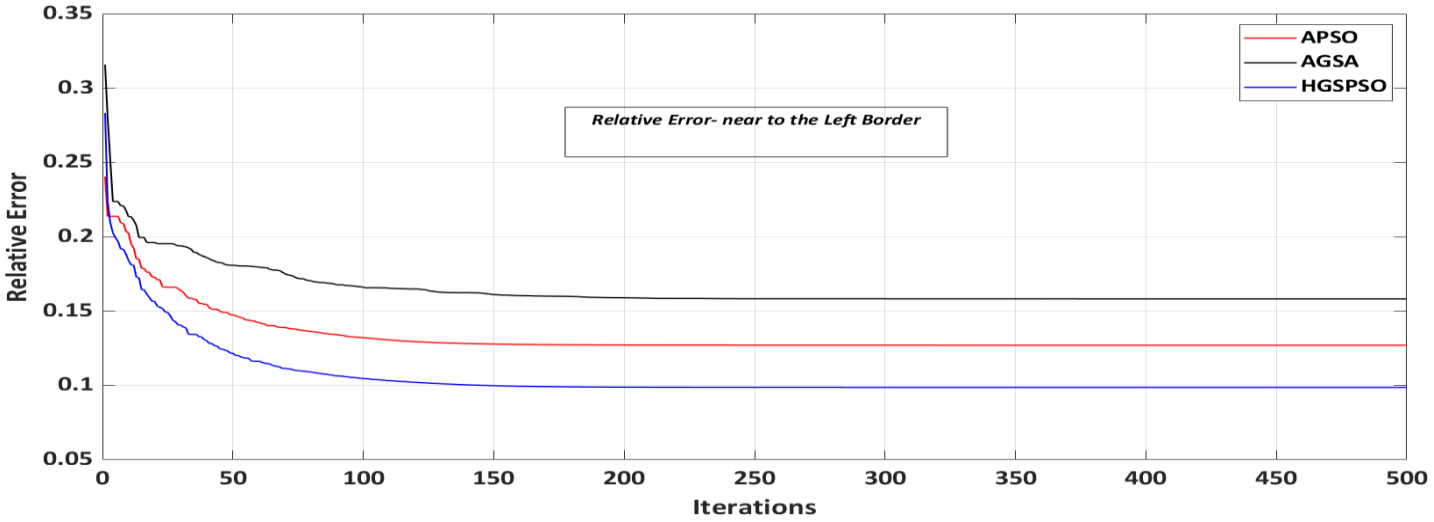

Figure 7 Error of reconstruction w.r.t iterations for an object placed at the left side of the circular tank

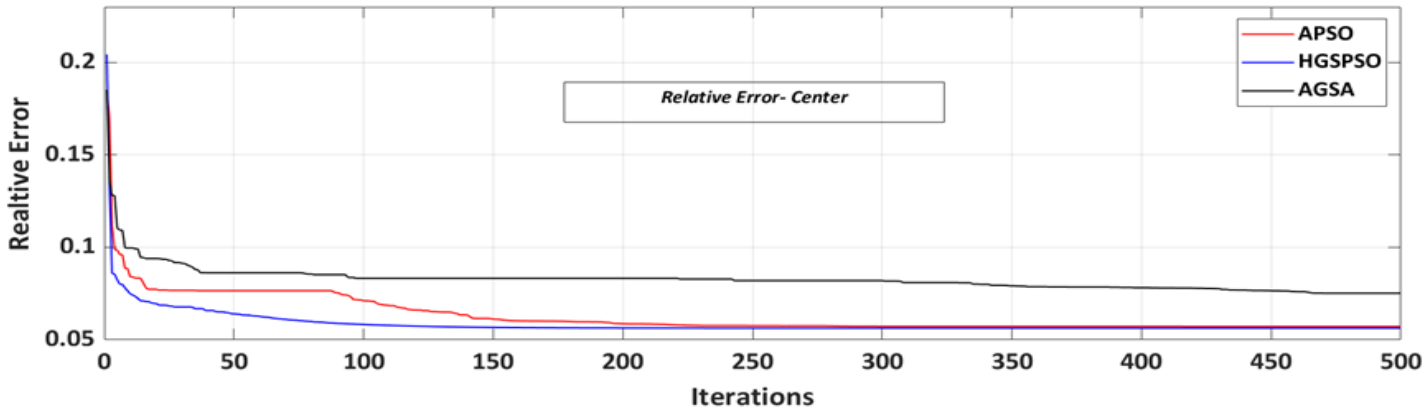

Figure 8 Error of reconstruction w.r.t iterations for an object placed at the centre of the circular tank

Table 2 Comparison of the proposed methods for the circular tank simulation

Case 1		HGSPSO	AGSA	APSO
Left	Mean	0.105967	0.16214	0.12699
	Std. Dev	0.011042	0.00279	0.000413
	Rank	***1***	3	2
Right	Mean	0.089787	0.128333	0.09883
	Std. Dev	0.000196	0.003377	0.000411
	Rank	***1***	3	2
Centre	Mean	0.055803	0.075223	0.058824
	Std. Dev	0.00045	0.000449	0.001092
	Rank	***1***	3	2

Table 2 compares the three proposed methods' mean and standard deviation values. It is clear from the table that the HGSPSO algorithm has lower values of the mean and standard deviation and has better performance than the other two techniques. The lower mean value of the reconstruction error shows that the reconstructed image matches the model better.

3.2 Gastroparesis (Case 2)

Gastroparesis is an illness that disturbs the stomach muscles and stops stomach emptying. Gastroparesis can affect digestion. The primary reason may be the damage to a nerve that controls the stomach muscles. Various pathological situations are related to delayed gastric emptying; common reasons are gastroparesis tributary to surgery, gastritis, diabetes, or gastric ulcer. Radionucleotide techniques, which encompass the classification of the solid or liquid phase of a meal with a standard isotope like ^{99}mTc and ^{111}In, are regarded as the most precise clinical methods for assessing gastric motility. This method involves ingesting a test meal followed by recurring imaging every 15 minutes for up to 3 hours to determine the commotion in the region of interest. The key factors that affect gastric motility are meal composition, volume, and caloric content.

Electrical impedance tomography (EIT) is a new medical imaging technology developed in the last few decades. It has three significant advantages: functional imaging, non-invasive, and medical image monitoring. Its benefits in the gastrointestinal field the most common application is to evaluate the flow of food through the stomach instead of the nuclide method, which is still regarded as the gold standard for gastric emptying measurement in clinical practice. EIT can accurately measure changes in gastric volume. EIT gastric emptying measurement correlates well with dye dilution, gastric retention, nuclide, etc. EIT gastric motility measurement uses electrodes placed on the body surface. The array realises non-destructive detection and directly displays the contraction and movement of the stomach body in the body in real-time image mode. It will significantly advance gastric motility detection and evaluation methods and show an attractive application prospect.

The stomach is one of the tissues and organs in the human body that are easier to extract EIT information. During the active period of the stomach, especially during the food digestion period, due to the contraction and movement of the stomach, its shape, volume, and content composition change significantly. The electrical characteristics change very; obviously, the signal is strong, and the information is enormous. The EIT technology can non-invasively and continuously detect the gastric motion signal, extract the electrical characteristics and change information corresponding to the gastric dynamics, and reflect the contraction, peristalsis, and emptying process to detect and evaluate gastric motility function.

3.2.1 Experimental Setup:

The experimental model for the gastric emptying problem consists of a cross-section of the human abdomen at the stomach level [18]. This model is available in the EIDORS library [19]. A sixteen electrodes EIT data acquisition system is used for measuring the voltage and injecting current. The system can detect applied voltage at all electrodes of a single injection pattern in 40ms. A current injection of 1 mA at 13 kHz was used. To disregard any conductivity modifications caused by cardiac activity, all the data was set at 100 ms. The conductivity distribution is then calculated by solving the nonlinear methodology of equations. The focus is mainly directed toward the dynamics of EIT due to its ability to overshadow minor measurement errors and sensitivity towards microscopic changes in conductivity. Electrodes were positioned uniformly, encompassing the subject's abdomen. The experiment was carried out three hours after the last meal the subject had consumed. A series of standardised values were obtained, and the subject drinking 355ml of Coke induced conductivity change. At intervals of five minutes, measurements were obtained for an hour. Based on this acquired data, conductivity changes with respect to changes in gastric activity were measured. Sixteen electrodes are placed at the periphery of the cross-section to simulate the real-world scenario.

The interior of the cross-section is modelled as a constant conductivity fluid. In contrast, the stomach is modelled as a circular region with constant conductivity, contrasting with the surroundings. The conductivity of the stomach varies with the number of contents inside it.

Figure 9 shows the experimental simulation setup for the gastric emptying problem. The number of electrodes can be increased if high-resolution images are required, increasing the computation time.

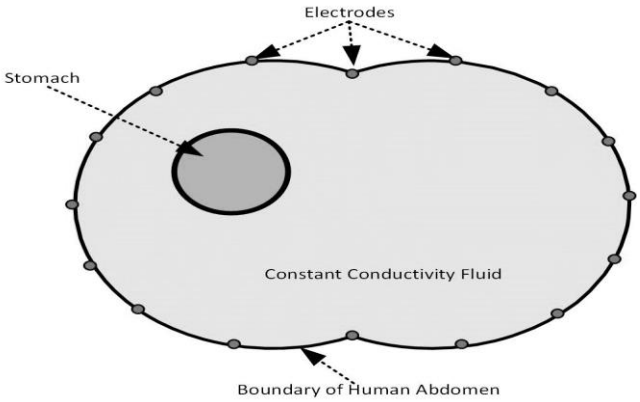

Figure 9 Experimental Model for Simulation of Gastric Emptying Problem

3.2.2 Results and Discussion

The parameters adopted for conducting the simulations for the three proposed algorithms are defined in Table 3.

Table 3 Parameters of the proposed methods for Case 2

Algorithms	Parameters
HGSPSO	Population size= 100, C_1 = [2.5-0.5], C_2= [0.5-2.5], w= (5.16), G_o=100
APSO	Population size=100, C_1 = [2.5-0.5], C_2= [0.5-2.5], w= (3.29)
AGSA	Population size=100, G_o=100

The data in this example is taken from the EIDORS-contributed data [20]. Figures 10-12, solved by the three proposed methods, present the variation in conductivity distribution between the reference calculations and those instantly after assimilation; the images taken after some time of the ingestion changed in amplitude only. In the left front section, there is an area of reduced conductivity that is similar to the position of the stomach. The sub-figures (*a*)-(*l*) in figures 10-12 show a gradual decrease in the conductivity in the stomach region with time. Figure (*a*) shows the image taken at the start of the process when the subject had ingested 330 ml of Coke. The data used in this study is taken from the EIDORS. Figure (*b*) shows the image captured after five minutes. All subsequent images (*c*)-(*l*) are captured at 5 minutes intervals. These figures show a reduction in the conductivity of the stomach. This is because as the drink leaves the stomach and enters the small intestine, the fluid inside the stomach decreases, reducing conductivity. The last figure (*l*) was captured 60 minutes after the subject had the drink. The stomach showed a lower conductivity than at the start of the gastric emptying test. All these sub-figures show a regressive decrease in the conductivity of the stomach. Fig 13 shows the relative error of reconstruction between the three proposed methods. The results indicate that the HGSPSO algorithm gives better image reconstruction with minimum error. This shows that EIT is subtle to conductivity variations if it lies away from the measurement plane as it detects the liquid even if it has gone into the small intestines and in the areas not possible by radionucleotide imaging. These results highlight that EIT is a promising physiological imaging technique.

Table 4 Comparison of the proposed methods for gastric emptying

Case 2	**HGSPSO**	**AGSA**	**APSO**
Mean	0.007677	0.044774	0.023499
Std. Dev	0.002317	0.001302	0.005139
Rank	***1***	3	2

Table 4 compares the APSO, AGSA, and HGSPSO algorithms for gastric emptying. The mean and standard deviation values indicate that the HGSPSO performs significantly better than the other two methods for gastric emptying.

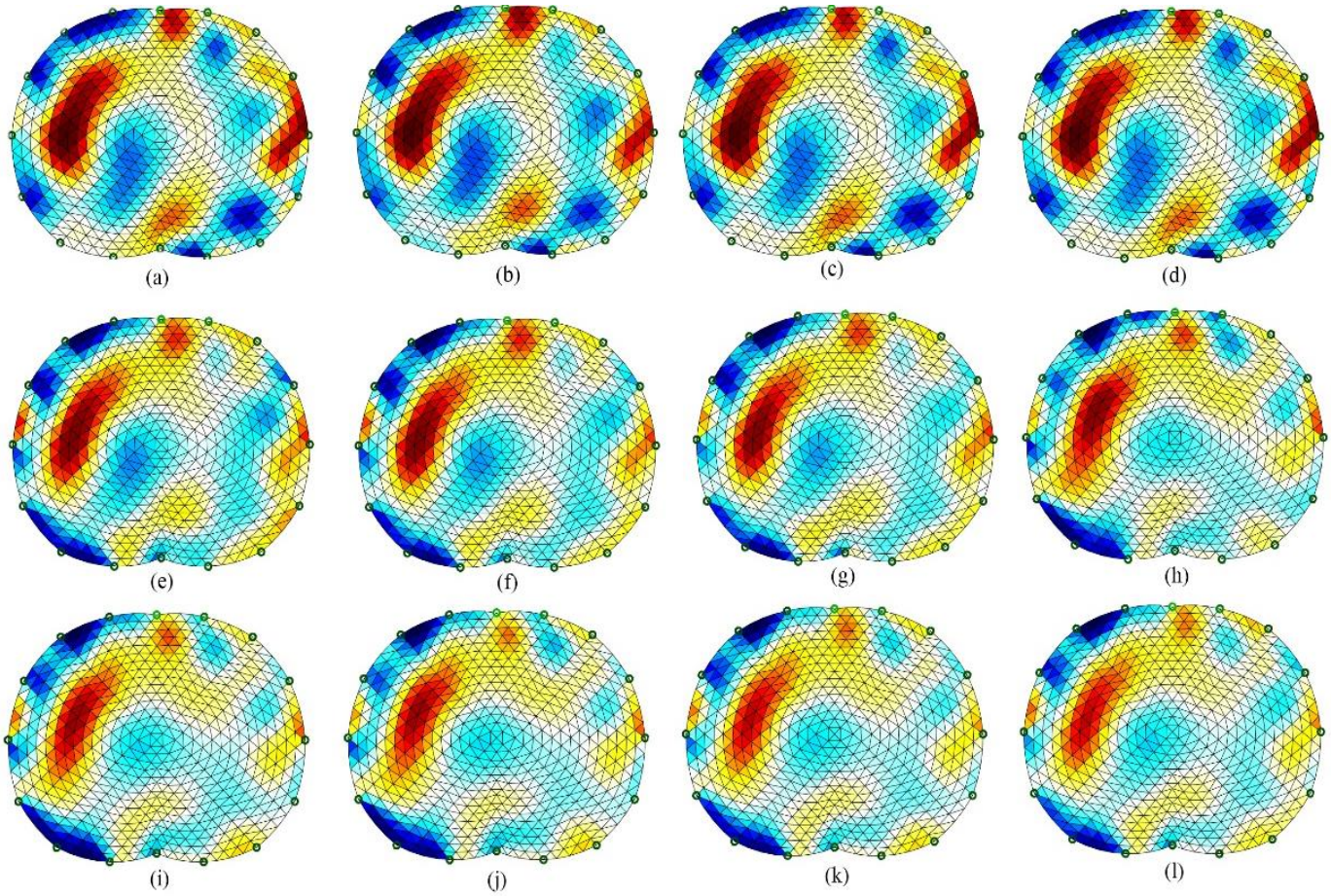

Figure 10 Gastric Emptying images by HGSPSO

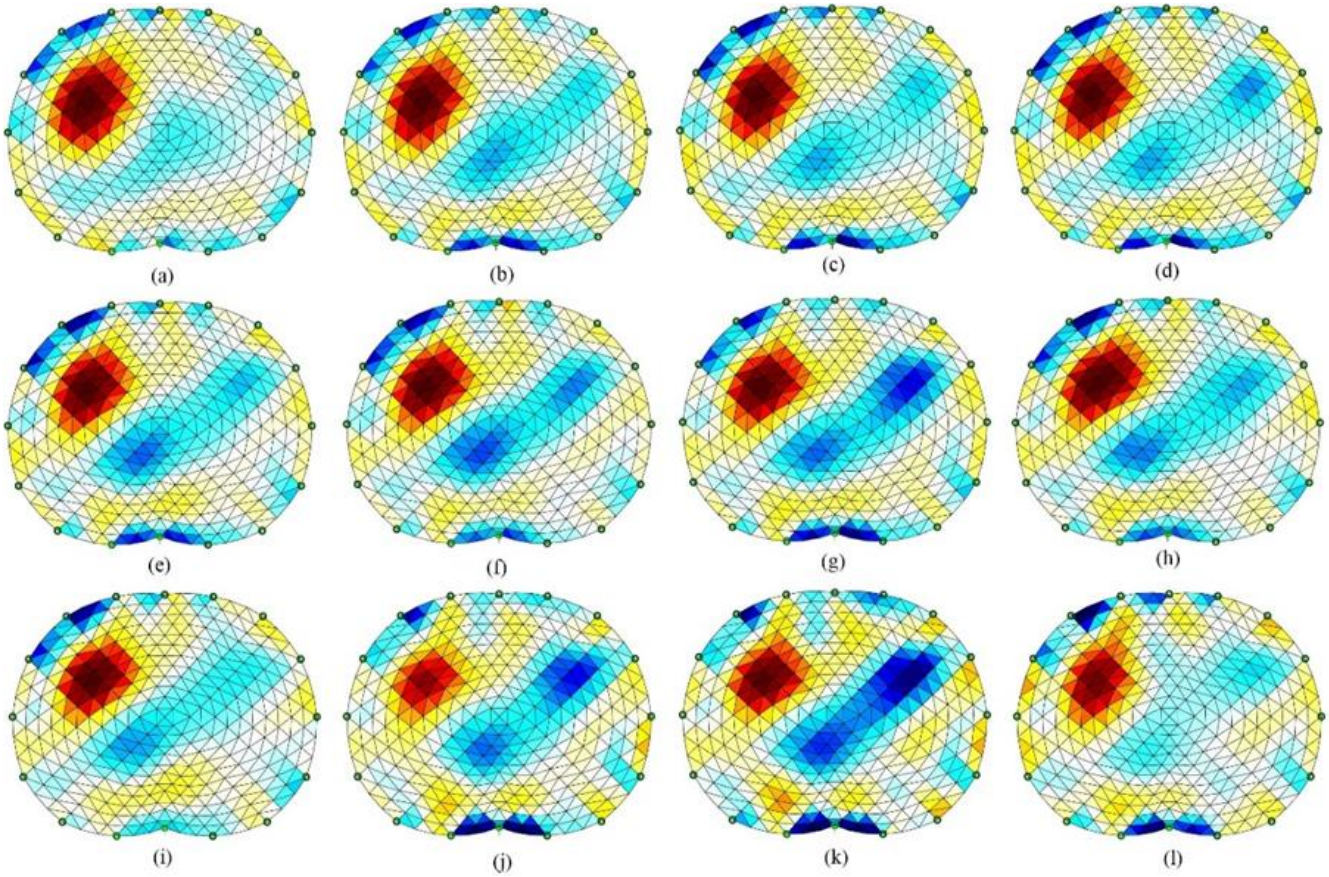

Figure 11 Gastric Emptying images obtained from AGSA

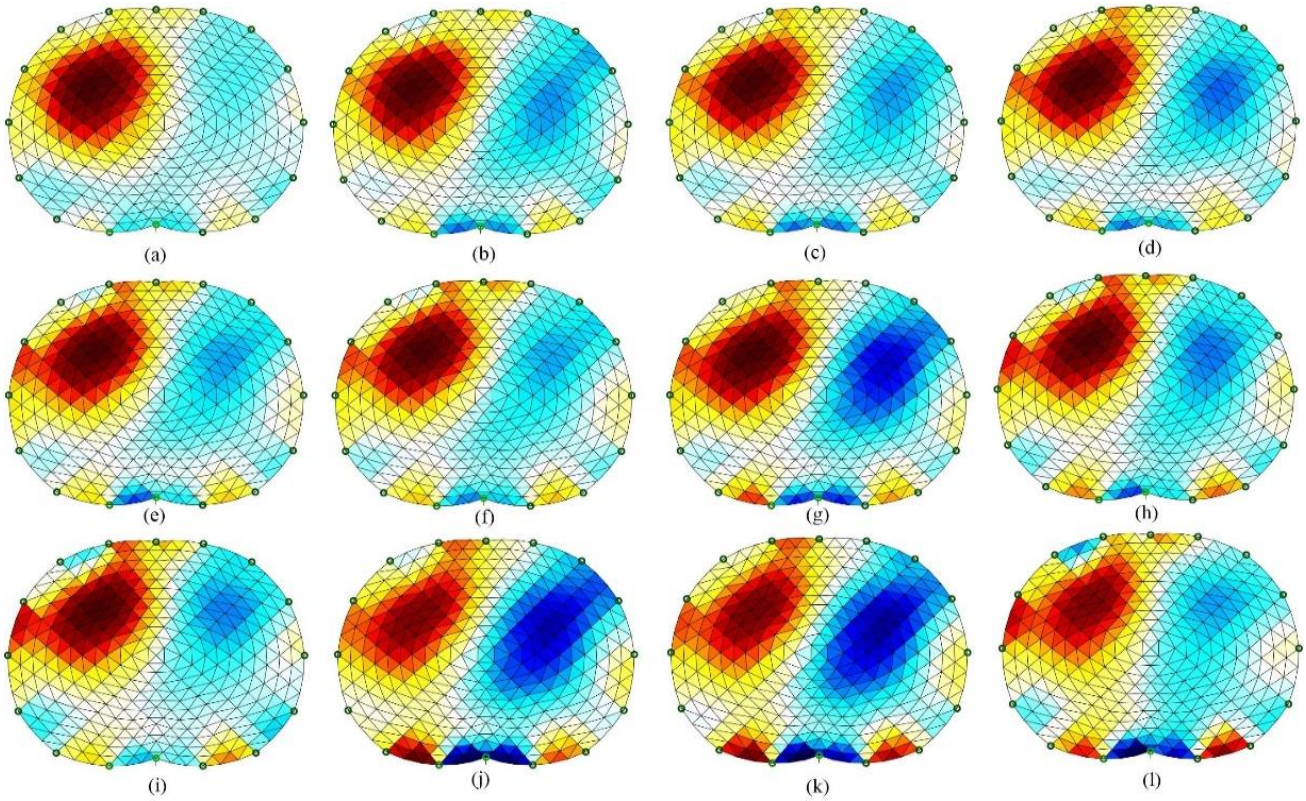

Figure 12 Gastric Emptying images obtained from APSO

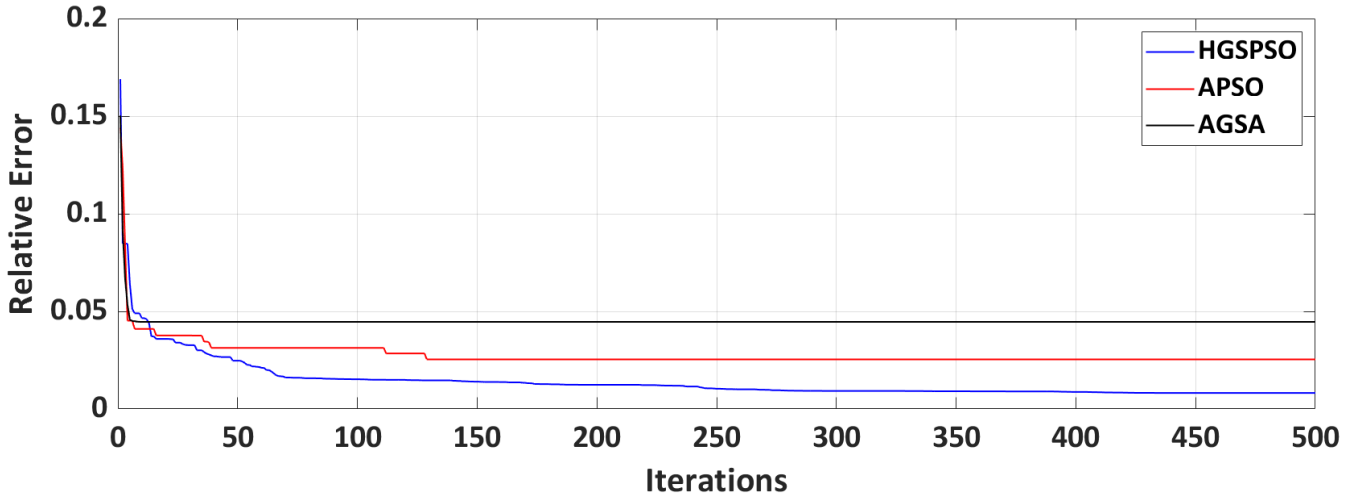

Figure 13 Comparison of the Relative Error of reconstruction between three proposed methods

4 Conclusions

The circular tank simulation is conducted using EIDORS. The forward model is built by FEM, where the circular domain is discretised into small elements. The proposed methods solve the EIT problem as an optimisation problem by minimising the root mean square error. The results showed that the HGSPSO method gives better image reconstruction than the other presented methods. The error value obtained from the HGSPSO algorithm is close to zero, which indicates that there is significantly less error between the model and the reconstructed images obtained in case 1. In addition to the simulations performed for the circular tank in case 1, a gastric emptying problem is also examined in this study.

EIT has outstanding advantages of functional imaging, non-invasive and medical image monitoring, which is conducive to detecting and evaluating gastric motility and changes during digestion and digestion. The frequency of gastric contraction and peristalsis is about three times/min. For EIT, the real-time requirements of the system are not high, impedance information is easy to extract, and one of the better EIT application targets. EIT gastric motility measurement uses electrode arrays placed on the body surface to achieve non-destructive testing and directly display the contraction of the gastric body in the body in real-time images. Identifying and eliminating respiratory disturbances and exercise conditions is easy, which will be the most critical advancement in gastric motility detection and evaluation methods, showing attractive application prospects.

The proposed methods give a new paradigm for solving the EIT problem. These methods not only optimise the reconstruction error of the EIT image but may also be used to enhance other features. There are several factors on which the reconstruction and forward problems are dependent. These factors include the signal-to-noise ratio, spatial resolution, and on modelling. Using population-based methods, these factors can be quickly and accurately optimised. The advantage of population-based methods is finding the best image out of many possibilities. These methods can also improve the resolution of the captured images. It can also optimise the voltage difference norm used for the time difference EIT image reconstruction.

Author contributions T.A.Khan wrote the main manuscript, S.A, Rizvi and S.Ling reviewed the work, T.A.Khan prepared the figures and pseudocodes, S.A.Rizvi and T.A.Khan have made a substantial contribution to the concept or design of the article, S. Ling has done supervision. All the authors have reviewed the final manuscript.

Funding: No funding is associated with this research.

Declaration

Conflict of interest: The authors declare no competing interests.

References

[1] A.M. Wicaksono, Basari, Design of Electrical Impedance Tomography (EIT) for Medical Imaging Application, 2019 IEEE 6th Int. Conf. Smart Instrumentation, Meas. Appl. ICSIMA 2019. (2019) 9057297. https://doi.org/10.1109/ICSIMA47653.2019.9057297.

[2] B. Amm, T.J. Kao, X. Wang, G. Boverman, D. Shoudy, J. Sabatini, J. Ashe, J. Newell, G. Saulnier, D. Isaacson, D. Davenport, Real-time 3D electrical impedance imaging for ventilation monitoring of the lung: Pilot study, Annu. Int. Conf. IEEE Eng. Med. Biol. Soc. IEEE Eng. Med. Biol. Soc. Annu. Int. Conf. 2014 (2014) 6064–6067. https://doi.org/10.1109/EMBC.2014.6945012.

[3] Z. Zhu, Y. Wang, Simultaneous Reconstruction of Conductivity and Permittivity in Electrical Impedance Tomography, Proc.

31st Chinese Control Decis. Conf. CCDC 2019. (2019) 3211–3215. https://doi.org/10.1109/CCDC.2019.8833397.

[4] N. Vaquero-Gallardo, H. Martínez-García, Electrical Impedance Tomography for Hand Gesture Recognition for HMI Interaction Applications, J. Low Power Electron. Appl. 2022, Vol. 12, Page 41. 12 (2022) 41. https://doi.org/10.3390/JLPEA12030041.

[5] Y. Wu, F.F. Hanzaee, D. Jiang, R.H. Bayford, A. Demosthenous, Electrical Impedance Tomography for Biomedical Applications: Circuits and Systems Review, IEEE Open J. Circuits Syst. 2 (2021) 380–397. https://doi.org/10.1109/OJCAS.2021.3075302.

[6] Y. Wu, D. Jiang, R. Yerworth, A. Demosthenous, An Imaged Based Method for Universal Performance Evaluation of Electrical Impedance Tomography Systems, IEEE Trans. Biomed. Circuits Syst. 15 (2021) 464–473. https://doi.org/10.1109/TBCAS.2021.3094773.

[7] T.A. Khan, S.H. Ling, Review on Electrical Impedance Tomography: Artificial Intelligence Methods and its Applications, Algorithms 2019, Vol. 12, Page 88. 12 (2019) 88. https://doi.org/10.3390/A12050088.

[8] J.L. Mueller, S. Siltanen, Chapter 16: Other direct solution methods for EIT, Comput. Sci. Eng. (2012) 249–279. https://doi.org/10.1137/1.9781611972344.CH16.

[9] A. Borsic, B.M. Graham, A. Adler, W.R.B. Lionheart, In vivo impedance imaging with total variation regularisation, IEEE Trans. Med. Imaging. 29 (2010) 44–54. https://doi.org/10.1109/TMI.2009.2022540.

[10] V. Kolehmainen, E. Somersalo, P.J. Vauhkonen, M. Vauhkonen, J.P. Kaipio, A Bayesian approach and total variation priors in 3D electrical impedance tomography, (2002) 1028–1031. https://doi.org/10.1109/IEMBS.1998.745625.

[11] X. Li, Y. Zhou, J. Wang, Q. Wang, Y. Lu, X. Duan, Y. Sun, J. Zhang, Z. Liu, A novel deep neural network method for electrical impedance tomography, Https://Doi.Org/10.1177/0142331219845037. 41 (2019) 4035–4049. https://doi.org/10.1177/0142331219845037.

[12] M.Y. Chen, G. Hu, W. He, Y.L. Yang, J.Q. Zhai, A reconstruction method for electrical impedance tomography using particle swarm optimisation, Lect. Notes Comput. Sci. (Including Subser. Lect. Notes Artif. Intell. Lect. Notes Bioinformatics). 6329 LNCS (2010) 342–350. https://doi.org/10.1007/978-3-642-15597-0_38/COVER.

[13] R. Hrabuska, M. Prauzek, M. Venclikova, J. Konecny, Image Reconstruction for Electrical Impedance Tomography: Experimental Comparison of Radial Basis Neural Network andGauss–Newton Method, IFAC-PapersOnLine. 51 (2018) 438–443. https://doi.org/10.1016/J.IFACOL.2018.07.114.

[14] T.A. Khan, S.H. Ling, A.S. Mohan, Advanced Particle Swarm Optimization Algorithm with Improved Velocity Update Strategy, Proc. - 2018 IEEE Int. Conf. Syst. Man, Cybern. SMC 2018. (2019) 3944–3949. https://doi.org/10.1109/SMC.2018.00669.

[15] T.A. Khan, S.H. Ling, A.S. Mohan, Advanced gravitational search algorithm with modified exploitation strategy, Conf. Proc. - IEEE Int. Conf. Syst. Man Cybern. 2019-October (2019) 1056–1061. https://doi.org/10.1109/SMC.2019.8914478.

[16] T.A. Khan, S.H. Ling, A novel hybrid gravitational search particle swarm optimisation algorithm, Eng. Appl. Artif. Intell. 102 (2021) 104263. https://doi.org/10.1016/J.ENGAPPAI.2021.104263.

[17] A. Adler, W.R.B. Lionheart, Uses and abuses of EIDORS: An extensible software base for EIT, (2006). http://eprints.maths.manchester.ac.uk/.

[18] A. Adler, R. Guardo, Y. Berthiaume, IMAGING OF GASTRIC EMPTYING WITH ELECTRICAL IMPEDANCE TOMOGRAPHY, (1994).

[19] A. Adler, W.R.B. Lionheart, EIDORS: Towards a community-based extensible software base for EIT | Request PDF, (2005). https://www.researchgate.net/publication/246037251_EIDORS_Towards_a_community-based_extensible_software_base_for_EIT.

[20] A. Adler, R. Guardo †, Y. Berthiaume, Imaging of gastric emptying with electrical impedance tomography, (2020).